MICROSCOPY RESEARCH AND TECHNIQUE 44:378–386 (1999)

Three-Dimensional High-Resolution Particle Tracking for Optical Tweezers by Forward Scattered Light

A. PRALLE, M. PRUMMER, E.-L. FLORIN,* E.H.K. STELZER, AND J.K.H. HÖRBER
European Molecular Biology Laboratory, D-69117 Heidelberg, Germany

KEY WORDS Brownian motion; optical tweezers; laser trap; optical interference; photonic force microscope (PFM); three-dimensional detector; single-particle tracking (SPT)

ABSTRACT A quadrant photodiode placed in the back-focal plane of the microscope of a laser trap provides a high-resolution position sensor. We show that in addition to the lateral displacement of a trapped sphere, its axial position can be measured by the ratio of the intensity of scattered laser light to the total amount of the light reaching the detector. The addition of the axial information offers true three-dimensional position detection in solution, creating, together with a position control, a photonic force microscope with nanometer spatial and microsecond temporal resolution. The measured position signals are explained as interference of the unscattered trapping laser beam with the laser light scattered by the trapped bead. Our model explains experimental data for trapped particles in the Rayleigh regime (radius $a < 0.2\lambda$) for displacements up to the focal dimensions. The cross-talk between the signals in the three directions is explained and it is shown that this cross-talk can be neglected for lateral displacements smaller than 75 nm and axial displacements below 150 nm. The advantages of three-dimensional single-particle tracking over conventional video-tracking are shown through the example of the diffusion of the GPI-anchored membrane protein Thy1.1 on a neurite. *Microsc. Res. Tech. 44:378–386, 1999.*

INTRODUCTION

In 1986, Ashkin and coworkers (Ashkin et al., 1986) showed that micrometer-size dielectric particles can be trapped optically in three dimensions in a single gradient laser trap. Since then, it has been demonstrated that particles as small as 25 nm in diameter can be manipulated (Block, 1992), intercolloidal interactions are observable (Crocker and Grier, 1994), forces generated by molecular motors can be measured (Svoboda et al., 1993), and changes in the diffusion of trapped particles near surfaces can be studied (Crocker, 1997; Pralle et al., 1998). Because of the harmonic nature of the trapping potential for small displacements, the force acting on the trapped bead can be measured by its displacement from the resting position within the trap. To measure small forces in the piconewton range using the optical trap, the displacement of the probe from the trapping position must be known precisely. Several detectors have been developed: an interferometer using the polarization of the laser light to measure lateral displacements along one axis (Svoboda et al., 1993), a confocal device measuring the two-photon fluorescence intensity emitted by a bead containing fluorophore to determine the axial displacement (Florin et al., 1996), and a photodiode placed behind the condenser (Denk and Webb, 1990; Ghislain, 1994) to measure lateral displacements. The latter two are more sensitive along one axis but the actual signal is a convolution of the three-dimensional displacement. The detection principle used commonly measures small lateral displacements in the focal plane with a quadrant photodiode (QPD*) placed in the back-focal plane (BFP) of the condenser (Allersma et al., 1998; Finer et al., 1994; Svoboda and Block, 1994). It provides the position of the trapped object with nanometer resolution and a bandwidth up to several MHz only limited by the performance of the photodiode and the amplifying electronics. Therefore, the sensor can be used to analyze thermal position fluctuations of trapped spheres, as long as laser power fluctuations and other noise sources, e.g., shot noise (low because of high laser intensity), are kept small.

To measure molecular forces, distances and movements in space precisely, the axial and the lateral position of the trapped particle have to be determined simultaneously to avoid ambiguities induced by the projection of the displacement on one or two axes. Here we show that the QPD placed in the BFP of the condenser also yields information about the axial position of trapped spheres, allowing them to be tracked in all three dimensions (3D). It enables the study of the three-dimensional diffusion of a particle confined in the trapping potential. A nice example for the use of the QPD for two-dimensional particle tracking in the focal plane is the study of the motion of a sphere dragged by the molecular motor NCD by Allersma (Allersma et al., 1998). But in many cases, the projection into a plane is not sufficient as we show here on the diffusion of the GPI-anchored membrane protein Thy1.1 in the plasma membrane of a neurite in three dimensions.

The mechanism of the position sensitivity of a QPD in the BFP had been unclear until, recently, a one-

*Abbreviations used: BFP = back-focal plane; DIC = differential interference contrast; GPI = glycosyl-phosphatylinositol; PFM = photonic force microscope; QPD = quadrant photodiode; SPT = single-particle tracking.

Contract grant sponsor: German Science Foundation (DFG).

*Correspondence to: E.-L. Florin European Molecular Biology Laboratory, D-69117 Heidelberg, Germany.

Accepted 14 November 1998

dimensional theoretical description for the lateral displacement in the focal plane was given by Gittes and Schmidt (1998). The measured intensity changes are described as interference of the light scattered on the sphere with the non-interacting transmitted light. We demonstrate a new approach that allows us to tackle the general three-dimensional case.

POSITION SENSING USING THE FORWARD SCATTERED LIGHT

For the special case of a one-dimensional lateral displacement in the focal plane, Gittes and Schmidt (1998) have shown that the position signal measured with a QPD in the BFP is determined by the interference of the unscattered laser beam with the scattered light. Here we develop a model for the general case of an arbitrary but small displacement of the trapped bead in three dimensions, assuming: The trapped sphere is described as a Rayleigh scatterer (i.e., a dielectric sphere with a radius a much smaller than the wavelength λ). In the Born approximation (Born and Wolf, 1989), the finite size of the sphere is accounted for by assuming a polarizability $\alpha = a^3 n^2 (m^2 - 1)/(m^2 + 2)$, $m = n/n_s$ (n and n_s are the refractive indices of the sphere and the solvent) and the dielectric constant ϵ. The QPD detects the light scattered forward only in a small angle. The scattering cross-section is then independent of the polarization of the light (Jackson, 1975). The bead position $\mathbf{r}'$ is given in cylindrical coordinates (z', $\rho'^2 = x'^2 + y'^2$, $\varphi' = \arctan y'/x'$), while the interference of scattered and unscattered light is observed at point $\mathbf{r}$ in the spherical coordinates r, ϑ, φ around the optical axis (see Fig. 2). The propagating field is described as a Gaussian beam with the scalar wavenumber $k = |\vec{k}| = 2\pi n/\lambda$, the radius of the Gaussian beam $R(z) = z(1 + (z_0/z)^2)$, the beam-waist radius in the focal plane $w_0 = \sqrt{\lambda z_0/\pi}$ and its variation along the optical axis $w(z) = w_0\sqrt{1 + (z/z_0)^2}$, the Rayleigh length of the focus $z_0 = \pi w_0^2/\lambda$, and the phase $\zeta(z) = \arctan(z/z_0)$ (Saleh and Teich, 1991). Passing the focus, the field undergoes the Gouy-phase jump, resulting in a 90° phase shift between scattered and unscattered light in the far field. The Gaussian field becomes (Saleh and Teich, 1991)

$$E(\mathbf{r}) = E_0 \frac{w_0}{w(z)} \exp\left\{-\frac{\rho^2}{w^2(z)}\right\} \cdot \exp\left\{-ikz - ik\frac{\rho^2}{2R^2(z)} + i\zeta(z)\right\}. \quad (1)$$

In the detection plane far from the focus ($r \gg z_0$) with the approximations $\zeta(z) = \arctan z/z_0 \approx \pi/2$, $w(z) \approx w_0 z/z_0$, $\sin\vartheta \approx \vartheta$, $z \approx r$, and $R(z) \approx \infty$ the unscattered field is

$$E(\mathbf{r}) \approx iE_0 \frac{kw_0}{2r} \exp\left[-ikr - \frac{1}{4}k^2 w_0^2 \vartheta^2\right], \qquad (r \gg z_0) \quad (2)$$

normalized by $E_0 = 2/(w_0\sqrt{\pi\epsilon_s c_s})$ onto total intensity $I_{tot} = 1$, with c_s the speed of light in the solvent. If a particle with polarizability α is placed at a lateral position $\mathbf{r}'$ near the geometric focus, the Rayleigh approximation for the scattered field at large $\mathbf{r}$ ($|\mathbf{r}| \gg z_0$) is

$$E(\mathbf{r}, \mathbf{r}') \approx \frac{k^2\alpha}{r} E(\mathbf{r}') \exp\left[ikr|\mathbf{r} - \mathbf{r}'|\right]. \quad (3)$$

The relative change in the time-averaged light intensity I due to the interference between the laser beam and the scattered light after subtraction of the offset $|E|^2$ is

$$\delta I = \frac{\epsilon_s c_s}{2}\{|E + E'|^2 - |E|^2\} \approx \epsilon_s c_s \,\mathrm{Re}\,\{EE'\}, \quad (4)$$

with $1/2\ |E + E'|^2$ being the time-averaged squared real part of the sum $(E + E')e^{-i\omega t}$, and $|E'|^2 \to 0$, ignoring any higher order interference. Using eqs. (2) and (3) the intensity change in the BFP for a displacement $\mathbf{r}'$ of the bead from the focus with $r = |\mathbf{r}|$, $r' = |\mathbf{r}'|$ becomes

$$\frac{\delta I(\mathbf{r}, \mathbf{r}')}{I_{tot}} = J(\mathbf{r}, \mathbf{r}') \sin\left[k\left(r - |r - r'| - z' - \frac{\rho'^2}{2R(z')} + \frac{\zeta(z')}{k}\right)\right], \quad (5)$$

$$\text{with } J(\mathbf{r}, \mathbf{r}') = \frac{2k^3\alpha}{\pi r^2}\left(1 + \left(\frac{z'}{z_0}\right)^2\right)^{-1/2} \cdot \exp\left[-\frac{\rho'^2}{w^2(z')}\right] \cdot e^{-k^2 w_0^2 \vartheta^2/4}. \quad (6)$$

The angle β between $\mathbf{r}$ and $\mathbf{r}'$ is given by

$$\cos\beta = \frac{\mathbf{r}\cdot\mathbf{r}'}{|\mathbf{r}|\,|\mathbf{r}'|} = \sin\vartheta\sin\vartheta'\cos\varphi\cos\varphi' + \sin\vartheta\sin\vartheta'\sin\varphi\sin\varphi' + \cos\vartheta\cos\vartheta'. \quad (7)$$

Because for small displacements $r'\sin\beta \ll r$, we substitute $r - |r - r'| \approx r'\cos\beta$. The relative change in the time-averaged light intensity I due to interference from eq. (5), simplified with $\psi' = \arctan(z'/\rho') = \pi/2 - \vartheta'$, $\chi = \varphi' - \varphi$ and $\cos\vartheta \approx 1$, becomes then

$$\frac{\delta I(\mathbf{r}, \mathbf{r}')}{I_{tot}} = J(\mathbf{r}, \mathbf{r}') \sin\left[k\left(r'\cos\psi'\sin\vartheta\cos\chi + r'\sin\psi' - z' - \frac{\rho'^2}{2R(z')} + \frac{\zeta(z')}{k}\right)\right]. \quad (8)$$

The interference pattern is observed by a QPD, so for all signals the change in intensity $\delta I/I$ is integrated over the space angle $\vartheta\varphi$. The angle ϑ runs from 0 to ϑ_{max}, where ϑ_{max} can be set to infinity since $\delta I/I$ decays

exponentially in ϑ. The z-signal is the total intensity, so χ covers all angles:

$$\frac{I_z}{I} = \int_0^{2\pi} d\chi \int_0^{\vartheta_{max}} d\vartheta r^2 \sin\vartheta \frac{\delta I(\mathbf{r}, \mathbf{r}')}{I_{tot}}. \quad (9)$$

The lateral signal is a result of the difference signal between any two halves. Because of $\delta I_+ = -\delta I_-$ it is sufficient to integrate the left half-space and the top half-space ($-\pi/2 < \chi < \pi/2$ and $0 < \chi < \pi$) for the x- and the y-signal, respectively. The integrations are performed analytically with the small angle approximation ($\sin\vartheta \approx \vartheta$). Then the lateral ($x$)-signal for a sphere at $\mathbf{r}' = \{x', y', z'\} = \{\rho', \varphi', z'\}$ is

$$\frac{I_x}{I}(\mathbf{r}') = I(z')\left[Ar'\cos\psi'\cos\varphi' + B\left(r'\sin\psi' - z' - \frac{\rho^2}{2R(z')} + \frac{\zeta(z')}{k}\right)\right], \quad (10)$$

with $I(z') = 4k^4\alpha/\pi(1 + (z'/z_0)^2)^{-1/2} \cdot \exp[-\rho'^2/w^2(z')]$, $A = 4\sqrt{\pi}/k^3w_0^3$ and $B = 2\pi/k^2w_0^2$. For the y-signal $\cos\varphi'$ is replaced by $\sin\varphi'$. The axial z-signal for an arbitrary displacement $\mathbf{r}'$ is

$$\frac{I_z}{I}(\mathbf{r}') = \frac{2\pi}{k^2w_0^2} I(z')\left[r'\sin\psi' - z' - \frac{\rho^2}{2R(z')} + \frac{\zeta(z')}{k}\right]. \quad (11)$$

This general three-dimensional description is reduced for a purely lateral displacement in one direction ($y' = z' = 0$) to the one-dimensional result of Gittes and Schmidt (1998)

$$\frac{I_x}{I}(x') = \frac{16k\alpha}{\sqrt{\pi}w_0^2}\left(\frac{x'}{w_0}\right)\exp\left[-\left(\frac{x'}{w_0}\right)^2\right]. \quad (12)$$

In the two-dimensional case, for a displacement ρ' in the focal plane at an angle φ', the lateral x-signal is

$$\frac{I_x}{I}(\rho', \varphi') = \frac{16k\alpha}{\sqrt{\pi}w_0^2}\cos\varphi'\left(\frac{\rho'}{w_0}\right)\exp\left[-\left(\frac{\rho'}{w_0}\right)^2\right]. \quad (13)$$

The axial signal is described on the optical axis ($x' = y' = 0$, $\cos\vartheta \approx 1$) more exactly, if the sine-function is not approximated:

$$\frac{I_z}{I}(z') = \frac{8k\alpha}{\pi w_0^2}\left(1 + \left(\frac{z'}{z_0}\right)^2\right)^{-1/2}\sin\left(\arctan\frac{z'}{z_0}\right) \quad (14)$$

Cross-Talk of the Three Position Signals

Using these calculations the cross-talk between the signals can be estimated. The lateral x-signal on the optical axis ($\rho' = 0$) depends on any axial displacement z'

$$\frac{\partial}{\partial z}\left(\frac{I_x}{I}(\mathbf{r}')\right)_{\rho'=0} \propto \left(1 + \left(\frac{z'}{z_0}\right)^2\right)^{-1/2}. \quad (15)$$

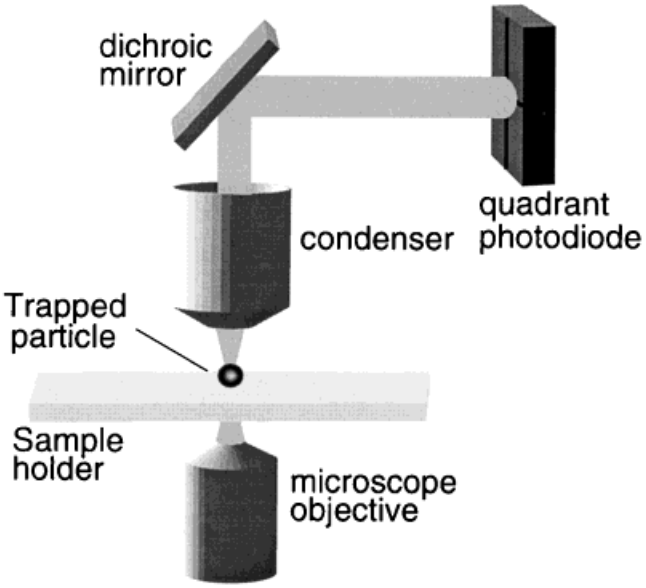

Fig. 1. Setup of the optical trap and the QPD in the BFP.

Using the value at $z' = 0$ for displacements of up to, e.g., $z' = 150$ nm this results in an underestimation of the x-displacement by less than 10%. The cross-talk of the two lateral signals x and y in the focal plane ($z' = 0$) is determined by their ratio $q = y/x$ and the absolute value in x

$$\frac{\partial}{\partial y}\left(\frac{I_x}{I}(\mathbf{r}')\right)_{z'=0} \propto \frac{q^2}{q^2+1}\exp\left[-\frac{(1+q^2)q^2}{w_0^2}\right]. \quad (16)$$

If a maximum underestimation of the displacement measurement of 10% is accepted, the detector response can be assumed to be linear up to lateral displacements of about $x = 100$ nm, as long as the y-displacement is smaller than 60 nm.

METHODS AND MATERIALS

Experimental Setup

Figure 1 shows the implementation of the laser trap in an inverted microscope (Axiovert 35, Zeiss Oberkoden, Germany) using the 1,064 nm line of a Nd:YVO_4 laser (T20-B10-106Q, Spectra Physics, Germany). The trapping laser is focused in the object plane by a high numerical aperture (NA = 1.3) oil-immersion microscope objective lens (Plan Neofluar 100×, Zeiss). The image of the condenser back focal plane is projected onto a quadrant photodiode (S5981, Hamamatsu, Herrsching, Germany) via a dichroic mirror (coated by DELTA Lys. & Optik, Denmark).

Measuring the Detector Response

The three-dimensional detector response was acquired by scanning the laser focus in a volume of 4 × 4 × 6 μm^3 across a fluorescent latex bead (radius $a = 300 \pm 19$ nm, FluoSpheres, Molecular Probes, Leiden, The Netherlands) adsorbed to the bottom cover-

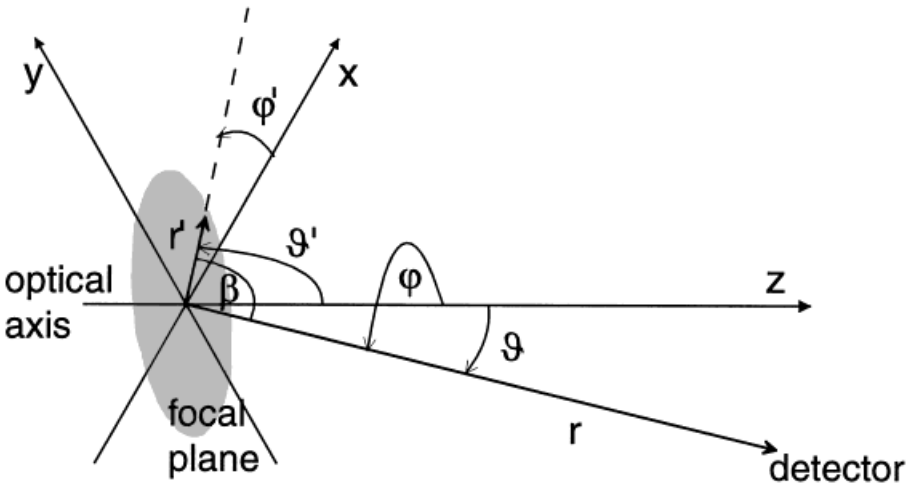

Fig. 2. Coordinates and angles used for the calculation. The laser beam is passing from the left, the bead placed at **r**′ near the focus and the detector at **r** to the right.

slip of the sample chamber while recording the intensity changes with the QPD. For the laser intensities used (about 50 mW in the focal plane), resulting in a lateral force constant of approximately 20 μN/m (calibrated using the Boltzmann distributed bead positions; Florin et al., 1998), the adsorption forces are much higher than the optical forces so that the bead's position remains uninfluenced by the trapping beam. The laser focus is moved along the optical axis by a piezo-driven microscope objective (P721.00, Physik Instrumente, Waldbronn, Germany) and perpendicular by a piezo-mounted scanning mirror (Piezosysteme Jena, Jena, Germany). The intensity changes at the QPD are recorded at $64 \times 64 \times 64$ points in the scanned volume using custom-made amplifiers and a data-acquisition board (AD-Win 5f, Jäger, Lorsch, Germany). The offset was subtracted and the amplitudes normalized to unity. Simultaneously, the two-photon fluorescence intensity emitted by the latex bead was recorded by a photomultiplier (R2949, Hamamatsu). Data analysis was performed using IgorPro (Wavemetrics, Lake Oswego, Oregon).

3D-Diffusion of Thy1.1

An example for the application of the detector three-dimensional single-particle tracking (3D-SPT) was performed on 7-day-old hippocampal neurons. These cells are extracted from 18-day-old rat embryos, plated on poly-l-lysine coated cover slips in a dish preincubated with glia cells, and grown at 37°C and 5% CO_2 in N_2-culture medium (Goslin and Banker, 1991). The experiments were carried out in the same medium, supplemented with 1% FSG (fish skin gelatine, Sigma-Aldrich, Dasenhofen, Germany) in a sealed chamber kept at 37°C. All media and solutions used were filtered through 0.1 μm SuporeAcrodisc filters (Gelman Sciences, Ann Arbor, MI). Orange fluorescent (530 nm/560 nm) latex beads (Fluo-Spheres, Molecular Probes, Leiden, The Netherlands) with a nominal diameter of 200 nm (actual diameter 216 nm ± 3.8%) were used as probe. Onto the spheres monoclonal antibodies against Thy1.1 were adsorbed, and blocked by FSG (according to Sako et al., 1998). The spheres were placed on the cells using the optical trap. After binding of the sphere to the membrane protein via the antibody, the trap stiffness was reduced to about 3.5 μN/m lateral and 0.5 μN/m axial.

Measuring Positions Using the Forward Scattered Light

The measured x-signal of the QPD for a sphere, 0.3 μm in radius, is shown in Figure 3. Figure 3a shows a xy-image-plot of the intensities measured in the focal plane. Overlaid are the contours of the fit obtained using the 2D-function eq. (13). The beam-waist radius w_0 in the focal plan is used as fit parameter, resulting in $w_{0x} = 0.33$ μm along the x-axis, and in $w_{0y} = 0.39$ μm along the y-axis (y-signal not shown). Figure 3b displays a profile of the data and the 2D-fit taken at zero displacement along the y-axis. It shows the good description of the signal by the theory up to displacements in the order of the focal dimension.

The axial displacement signal's dependence on simultaneous lateral and axial displacements is shown in Figure 4. Figure 4a displays a zx-image-plot of the intensities measured overlaid with the contours of the fit obtained using the 3D-function eq. (11) for $y = 0$. In addition to the beam-waist radius w_0 in the focal plane, the Rayleigh length z_0 is used as fit parameter resulting in $w_0 = 0.46$ μm and $z_0 = 0.73$ μm. Figure 4b displays a profile of the data and the 2D-fit taken at zero displacement along the optical-axis. In addition, the 1D-fit obtained by eq. (14) is plotted. The 2D-function describes the detector response up to displacements smaller than the focal dimension well. The small angle-approximation, which is necessary to perform the 2D-integration, induces discrepancies between the theory and the measurement for larger displacements. These are better explained by the 1D-function, which was calculated without the small angle-approximation.

Using beads filled with fluorophore, which is excited by the infrared trapping beam via a two-photon process, and measuring the intensity of the two-photon fluorescence simultaneously to the signal on the QPD, provides additional information about the beam focus. Figure 5 displays cuts across the focus laterally (Fig. 5a) and along the optical axis (Fig. 5b). The intensities are normalized, and the square-root is taken because of the

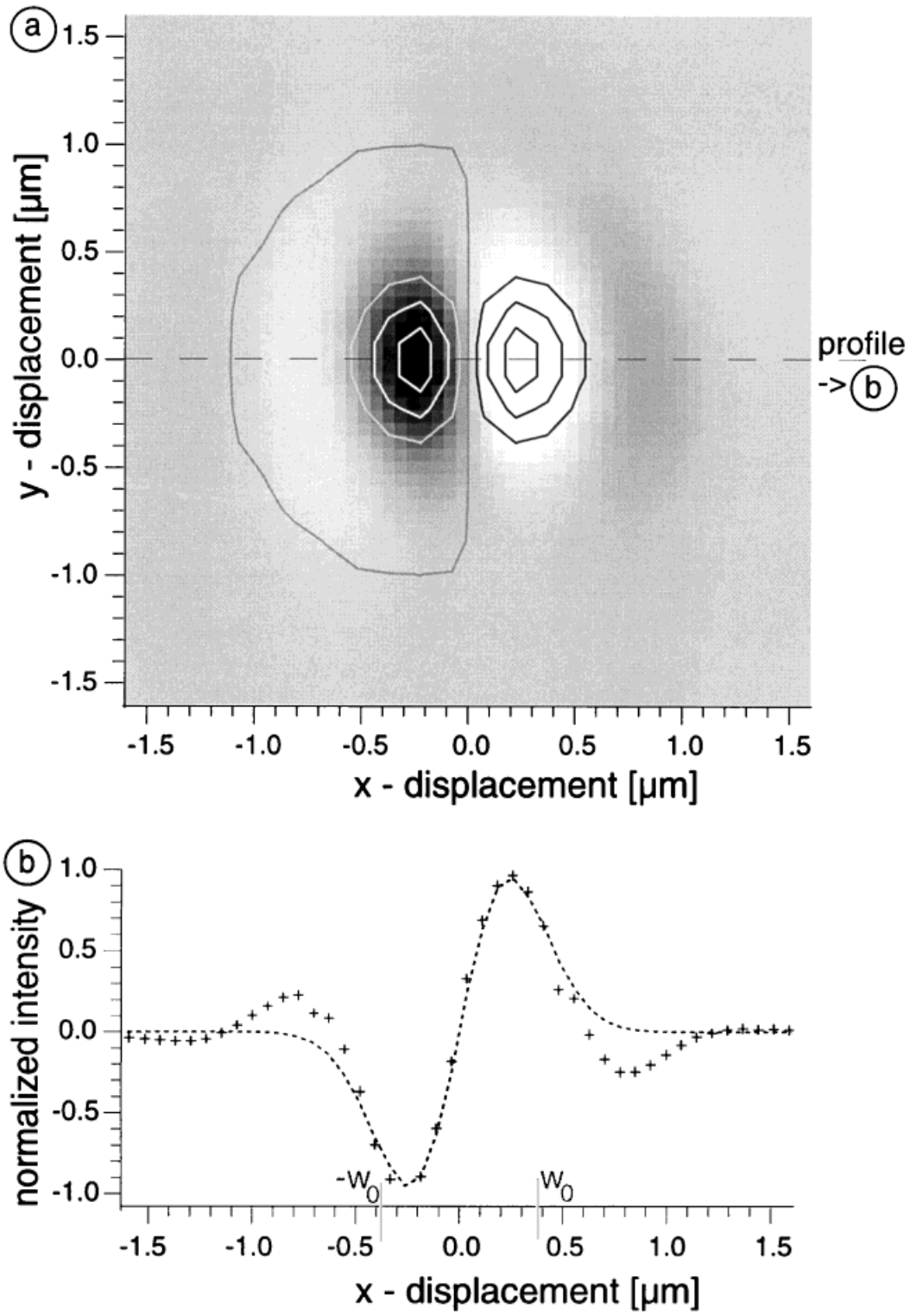

Fig. 3. **a:** Slice (x,y) of the measured lateral position signal in the focal plane shown as image plot. The theoretical predictions are plotted as contour lines. **b:** Linear profiles along the x-axis, zero y-displacement, of the measured response (+) and the 2D-fit function with $w_0 = 0.33$ µm.

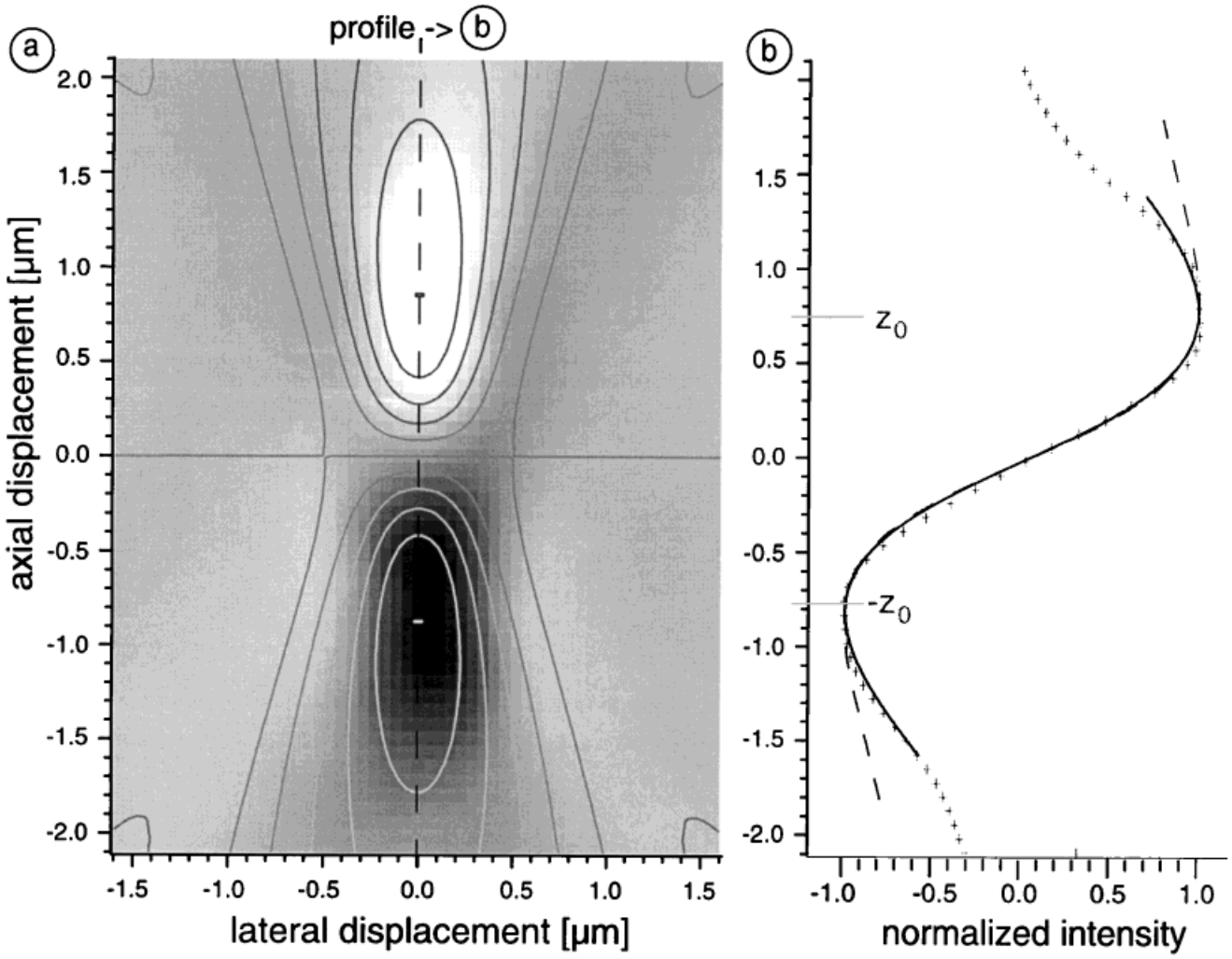

Fig. 4. **a:** Slice (z,x) of the measured axial position signal shown as image plot. The theoretical predictions are plotted as contour lines. **b:** Linear profiles along the optical axis of the measured response (+), the 2D-fit (dashed line) and the 1D-fit functions (cont. line) with $z_0 = 0.76$ µm.

two-photon excitation, obtaining the focal dimensions $w_{0f} = 0.57$ µm and $z_{0f} = 0.64$ µm.

DISCUSSION OF THE POSITION SIGNAL

The theory describes the detected signals for small three-dimensional displacements of a trapped sphere within a few percent. The sphere is approximated by a point-like Rayleigh scatterer and only first-order interference is required to explain the measurements for displacements up to the focal dimensions w_0 and z_0 (see Figs. 3 and 4).

The model results in beam-waist radius w_0 and Rayleigh length z_0, corresponding well to the value expected for the used objective. For our objective lens with NA 1.3, one calculates a beam-waist radius $w_0 = 0.32$ µm and a Rayleigh length $z_0 = 0.55$ µm (S. Grill, private communication). Convoluting the expected focus with a sphere of 300 nm radius, the model predicts $w_{0f} = 0.48$ µm and $z_{0f} = 0.64$ µm. The agreement of the focal dimensions obtained from the scattering ($w_0 = 0.46$ µm and $z_0 = 0.73$ µm) and the two-photon fluorescence measurement ($w_{0f} = 0.57$ µm and $z_{0f} = 0.64$ µm) with these predictions supports the theory.

The detector is more sensitive to lateral displacements than to axial displacements. The lateral signal scales with the ratio of displacement to beam-waist radius: ρ / w_0, while the axial signal depends on the ratio of displacement to Rayleigh length: z / z_0. Even though both are in the range of the wavelength, the beam-waist radius is about two to three times smaller than the Rayleigh length. Therefore, the lateral sensitivity is about threefold higher than the axial sensitivity. As long as the axial displacement is small compared to the Rayleigh length ($z \leq 150$ nm) the lateral sensitivity can be assumed to be independent of the axial position, as the resulting underestimation would be smaller than 10%. According to eq. (15), the cross-talk between the two lateral directions is larger; according to eq. (16), it may be neglected for displacements predominately along one of the axes, but for

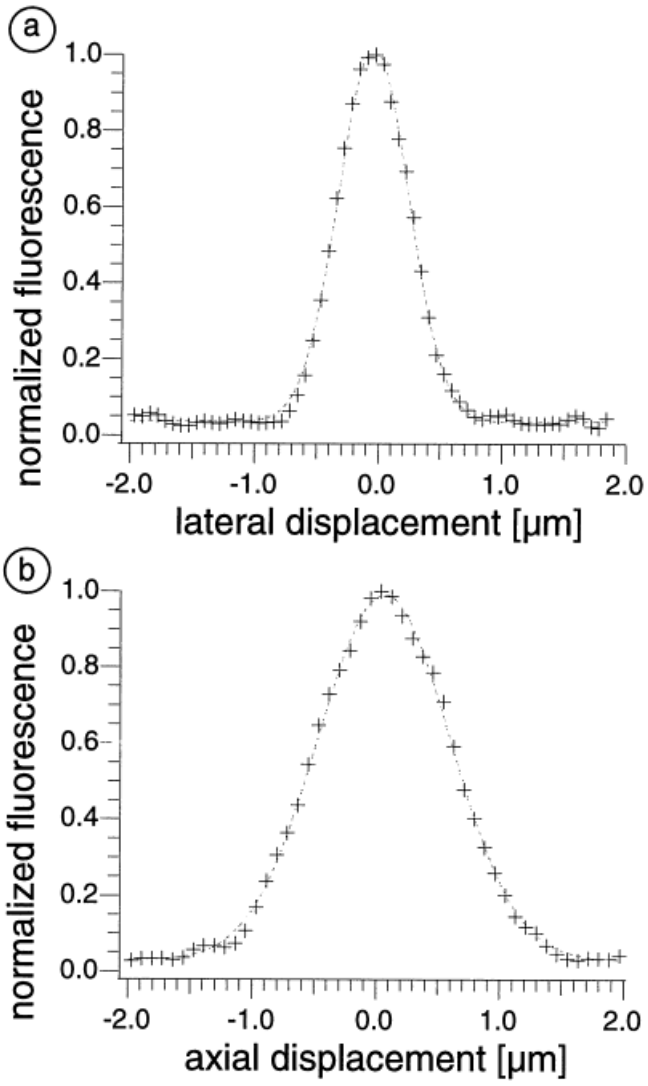

Fig. 5. Line profiles of the two-photon fluorescence intensities measured (+) when moving the focus across a 0.6 μm-diameter bead perpendicular (**a**) and along (**b**) the optical axis.

displacements at 45° to the axes, the underestimation of the position can reach 30%, if a linear sensitivity is assumed. For larger displacements, the cross-talk and the nonlinearities have to be corrected using either this theory or the previously measured detector response. The detector response has to be determined for each particle-size and trapping laser intensity used.

For ideal optics, the detection would be independent of the distance to the coverslip surface. But due to spherical aberrations of the trapping laser beam, it has to be calibrated near the point where it is used. Using the trapping laser as a source of the scattering provides the advantage that the area of highest sensitivity of the detector is automatically aligned with the resting position of the sphere in the trapping potential. The trapping laser provides enough intensity that low-noise detection and amplification are possible. But for small spheres, the amount of unscattered light becomes very large. This offset has to be subtracted from the signal (eq. (4)). In the lateral signal, the unscattered light is cancelled out by subtracting the signal of one half of the QPD from the other half. But the offset contributes a large part to the total intensity measured as axial position signal. Therefore, the axial position signal is prone to errors induced by laser power fluctuations and spherical aberration effects. This may hamper the signal considerably, especially for small spheres ($a < 100$ nm) for which the scattering cross sections become very small.

Because of these properties of the position signal, a QPD placed in the BFP of an optical trap allows three-dimensional tracking of a Brownian particle within the trapping region with a temporal and spatial resolution not achievable before. As an example for the high resolution achieved, we present the 3D-particle tracking of a membrane protein.

3D-PARTICLE TRACKING ON A NEURITE

Single-particle tracking (SPT), the study of the diffusion of plasma membrane components by the tracking of attached spheres using video-microscopy, has brought new insight into the dynamics of the plasma membrane (see, e.g., Sako and Kusumi, 1994; Jacobson et al., 1995). The use of video microscopy for SPT has limited the study to two dimensions and offered only low temporal resolution. A membrane protein with a diffusion coefficient of about $D = 1 \cdot 10^{-10}$ cm^2/s would move in an area of about $(200\ nm)^2$ around its origin in two subsequent video images (25 fps), which prohibits high spatial resolution. The development of fast cameras overcomes the temporal limitation partially. But, still, cameras only provide a 2D-projection, while cellular systems are three-dimensional structures. To study diffusion on such cells, three-dimensional information is important. We show here the application of a QPD placed in the BFP to track the motion of GPI-anchored membrane protein Thy1.1 over the surface of a neurite of a hippocampal neuron in three dimensions with high temporal resolution.

Figure 6 shows the three-dimensional tracking of a Thy1.1 molecule diffusing on the neurite membrane. The position was measured every 20 μs over a period of 42 s resulting in $2.1 \cdot 10^6$ data points. Figure 6a displays a surface representation of the volume in which the sphere has been diffusing during 85% of the time. The tubular outline of the neurite is clearly visible as the molecule is diffusing around it. Figure 6b shows the DIC (differential-interference contrast)-microscope view of the bead (marked by the white circle) on the neurite. For comparison with 2D-SPT the probabilities of the positions reached in the first 840 ms are shown in Figure 6c as a two-dimensional projection. The loss of the axial position converts tracks up and down on the side of the neurite into areas of high probability and apparent confinement (Fig. 6c, bottom right). To show the importance of the high temporal resolution, the tracks are displayed in (Fig. 6d) at reduced temporal

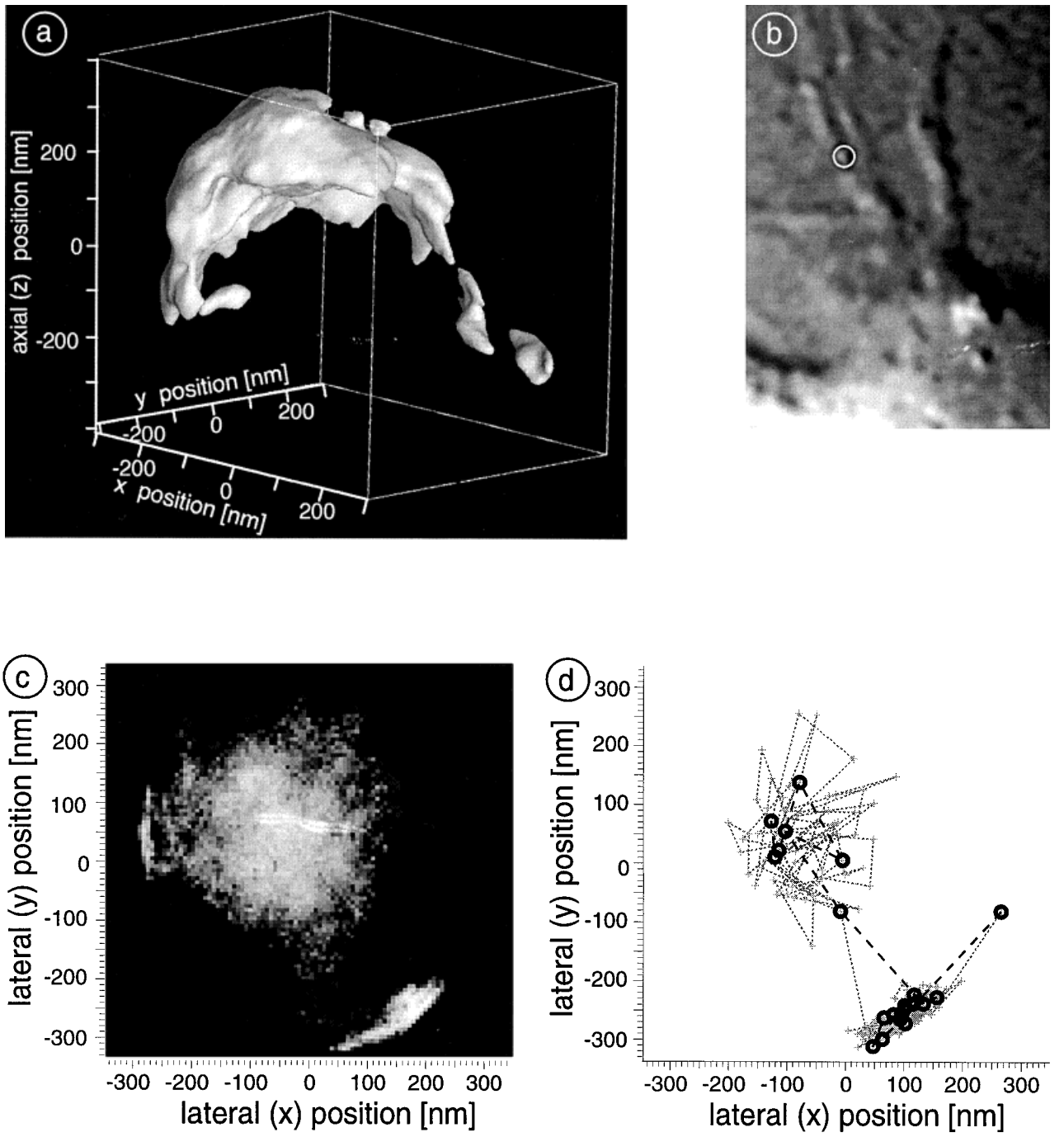

Fig. 6. 3D-SPT of a Thy1.1 molecule diffusing on the neurite membrane. **a:** Surface plot of the volume in which the molecule-bead complex is found 85% of the measurement time. **b:** DIC-image of the bead (marked by the white circle) on the neurite. **c:** 2D-projection of the probabilities of the positions reached in the first 840 ms. **d:** Tracks visible at the reduced temporal resolution of 4 ms (+++), and at normal video-camera speed (40 ms, 000).

resolution: with 4 ms (+++) resolution, and at normal video-camera speed (40 ms, 000). This example demonstrates the importance of the third dimension and the high temporal resolution (i.e., 20 μs). Because of the size of the neurite of about 0.2 μm in diameter, the measured positions have to be deconvoluted with the detector response function (eqs. (10) and (11)), and the influence of the weak potential of the optical trap has to be accounted for.

The possibility to perform three-dimensional single molecule tracking in the plasma membrane with superior temporal and spatial resolution, offers the chance to study the dynamics of a single membrane molecule at a scale not achievable before.

ACKNOWLEDGMENTS

We thank B. Hellias and C. Dotti for the hippocampal neurons. This work was partially supported by the German Science Foundation (DFG).

REFERENCES

Allersma M, Gittes F, deCastro MJ, Stewart RJ, Schmidt CF. 1998. Two-dimensional tracking of ncd motility by back focal plane interferometry. Biophys J 74:1074–1085.

Ashkin A, Dziedzic JM, Bjorkholm JE, Chu S. 1986. Observation of a single-beam gradient force optical trap for dielectric particles. Opt Lett 11:288–290.

Block SM. 1992. Making light work with optical tweezers. Nature 360:493–495.

Born M, Wolf E. 1989. Principles of optics, 6th ed. Oxford: Pergamon Press.

Crocker JC. 1997. Measurement of the hydrodynamic corrections to the brownian motion of two colloidal spheres. J Chem Phys 106:2837–2840.

Crocker JC, Grier DG. 1994. A microscopic measurement of the pair interaction potential of charge-stabilized colloid. Phys Rev Lett 73:352–355.

Denk W, Webb WW. 1990. Optical measurement of picometer displacements of transparent, microscopic objects. Appl Opt 29:2382–2391.

Finer JT, Simmons RM, Spudich JA. 1994. Single myosin molecule mechanics: piconewton forces and nanometer steps. Nature 368:113–118.

Florin E-L, Hörber JHK, Stelzer EHK. 1996. High resolution axial and lateral position sensing using two-photon excitation of fluorophores by a continuous Nd: YAG laser. Appl Phys Lett 69:446–448.

Florin E-L, Pralle A, Stelzer EHK, Hörber JHK. 1998. Photonic force microscope calibration by thermal noise analysis. Appl Phys A 66:S75–S78.

Ghislain LP, Switz NA, Webb WW. 1994. Measurement of small forces using an optical trap. Rev Sci Instrum 65:2762–2768.

Gittes F, Schmidt CF. 1998. Signals and noise in micromechanical measurements. Methods Cell Biol 55:129–132.

Goslin K, Banker G. 1991. Culturing nerve cells. Cambridge, MA: M.I.T. Press.

Jackson JD. 1975. Classical electrodynamics, 2nd ed. New York: John Wiley & Sons.

Jacobson K, Sheets ED, Simons R. 1995. Revisiting the fluid mosaic model of membranes. Science 268:1441–1442.

Pralle A, Florin E-L, Stelzer EHK, Hörber JHK. 1998. Local viscosity probes by photonic force microscopy. Appl Physiol A 66:S71–S73.

Sako Y, Kusumi A. 1994. Cytoplasmic regulation of the movement of E-cadherin on the free cell surface as studied by optical tweezers and single particle tracking: corralling and tethering by the membrane skeleton. J Cell Biol 125:1251–1264.

Sako Y, Nagafuchi A, Tsukita S, Masatoshi T, Kusumi A. 1998. Compartmentalized structure of the plasma membrane for receptor movements as revealed by a nanometer-level motion analysis. J Cell Biol 140:1227–1240.

Saleh BEA, Teich MC. 1991. Photonics. New York: John Wiley & Sons.

Svoboda K, Block SM. 1994. Biological applications of optical forces. Ann Rev Biophys Biomol Struct 23:247–285.

Svoboda K, Schmidt CF, Schnapp BJ, Block SM. 1993. Direct observation of kinesin stepping by optical trapping interferometry. Nature 365:721–727.